RSC Advances

PAPER

View Article Online
View Journal | View Issue

Cite this: *RSC Adv.*, 2024, **14**, 23840

Molecular dynamics simulation and experimental verification of the effects of vinyl silicone oil viscosity on the mechanical properties of silicone rubber foam†

Hongyu He,[ab] Lulu Li,[a] Ruhan Ya,[c] Hong Liu,[d] Bin Luo,[d] Zhipeng Li *[b] and Wenhuai Tian *[b]

The molecular motion trajectories of silicone rubber foam (SRF) at various vinyl silicone oil viscosities were studied *via* molecular dynamics (MD) simulation from the perspective of all atomic molecules. The influence of different viscosities of vinyl silicone oil on interaction, compatibility, and aggregation degree of molecules was determined based on the mean square displacement, diffusion coefficient, binding energy, solubility parameter, radial distribution function, and radius of gyration. The mechanical properties of the SRF were also experimentally verified. Results revealed that as the viscosity of vinyl silicone oil increased, the mean square displacement, fractional free volume, diffusion coefficient, and solubility parameter of the system decreased, whereas its larger radius of gyration increased. Moreover, the radial distribution function showed a weaker relative interaction between molecular chains. The calculated binding energy demonstrated that the system had better compatibility at a viscosity of 0.45 Pa s. This study provided a deeper insight into the relation between the viscosity of vinyl silicone oil and mechanical properties of the SRF. As the viscosity of vinyl silicone oil increased, the changing trend in MD simulation results of elastic modulus, shear modulus, bulk modulus, and Poisson's ratio was consistent with the experimental results. The MD simulations can promote theoretical predictions and scientific basis for the design of the SRF with desired performances.

Received 2nd July 2024
Accepted 17th July 2024

DOI: 10.1039/d4ra04784b

rsc.li/rsc-advances

1. Introduction

Silicone rubber foam (SRF) is widely applied in vehicles, high-speed trains, and airplanes owing to its low compression set, superior temperature resistance, and good resilience.[1–3] SRF is commonly foamed from silicone rubber matrix comprising polysiloxane, fillers, and other additives.[4] Chemical foaming technology is used to produce the SRF due to the characteristics of one-step and green process.[5] The viscosity of the matrix plays a crucial role in the cellular structure and properties of the SRF. For example, if the viscosity of vinyl silicone oil is considerably low or high, the polymer molecular chains will be shorter or longer, respectively, which have a significant impact on the performance of the SRF.[6,7]

Molecular dynamics (MD) is a method to simulate the properties of materials at the micromolecular and atomic levels. It is used to study the effects and mechanisms of polymer modification because a large number of atoms or molecules are simulated on a large time scale.[8–10] MD simulation explores the interactions between microscopic molecules based on the principle of statistical analysis of the arrangement and motion of atoms or molecules, which cannot be experimentally derived. Various polymer properties have been investigated *via* MD simulation.[11,12] Pahari *et al.*[11] found that MD simulation can be used to effectively predict the viscoelastic and thermodynamic properties of rubber. Lee *et al.*[12] utilized MD simulation to analyze the fibrillization process and thermal stability of silicone foams by adding fibrillated microcrystalline cellulose, and the simulation result of fibrillization details was consistent with the experimental result. Wei *et al.*[13] applied MD simulation method to investigate the mechanical properties of poly(vinyl alcohol) (PVA)/poly(acrylic acid) (PAA) blend systems. Results showed that the PVA chain formed a stronger intermolecular interaction than the PAA chain at the same quality. Zhu *et al.*[14] studied the dynamic mechanical property of silicone rubbers with different phenyl units and phenyl contents *via* combining experiments and MD simulation.

[a]*School of Materials Science and Engineering, University of Science and Technology Beijing, Beijing 100083, China. E-mail: hehongyu666@126.com; 15733153822@163.com*

[b]*School of Materials Science and Engineering, Shunde Innovation School, University of Science and Technology Beijing, Foshan 528300, China. E-mail: zplmse@ustb.edu.cn; wenhuaitian@ustb.edu.cn*

[c]*Inner Mongolia Academy of Science and Technology, Huhhot 010020, China. E-mail: YARUHANJIAN@163.com*

[d]*Guangdong Homeen Organic Silicon Material Co., Ltd, Zhaoqing 526072, China. E-mail: roben@hm-sil.com; liuhong@homeen.cn*

† Electronic supplementary information (ESI) available. See DOI: https://doi.org/10.1039/d4ra04784b

Currently, the regulation of cellular structure, rheology, viscoelasticity, and aging of the SRF have been studied.[15–19] Few researchers have conducted in-depth the impact of vinyl silicone oil viscosity on the performance of the SRF *via* all-atom molecular dynamic simulation.[20,21] This article has investigated in detail the molecular motion trajectories, molecular interactions, and the crosslinking process of the SRF prepared from vinyl silicone oil with different viscosities through MD simulation. The intermolecular motion (such as mean square displacement, diffusion coefficient, fractional free volume, and cohesive energy density) and the molecular stereo configuration (radial distribution function and radius of gyration) were also investigated. The simulation results of mechanical properties and the experimental results were in contrast with each other. This research will provide theoretical basis and data support for the actual industrial production of the SRF.

2. MD simulation and experiment

2.1 Materials

Vinyl-terminated silicone oils with vinyl group (purity ≥99%, viscosity = 0.45 Pa s, 10 Pa s and 200 Pa s) and vinyl-terminated MQ silicone resin (purity ≥99%, viscosity = 100 Pa s) were provided by Jiangxi Bluestar Xinghuo Silicones Co., Ltd (Jiujiang, China). Hydrogen-containing silicone oil (viscosity = 0.02 Pa s, purity ≥98%, active hydrogen mass fraction = 1.6%) was obtained from Zhejiang Runhe Organic silicone New Material Co., Ltd (Huzhou, China). Hydroxyl-terminated silicone oil (purity ≥98%, hydroxyl value = 5%, viscosity = 0.02 Pa s) was provided by Zhonghao Chenguang Research Institute of Chemical Industry Co., Ltd (Zigong, China). The platinum catalyst (Karstedt's catalyst, platinum mass fraction = 0.5%) was obtained from Tianjin Umicore Catalyst Co., Ltd (Tianjin, China). The inhibitor (1-ethynylcyclohexanol, purity ≥99%) was provided by Guangdong Silicon New Material Co., Ltd (Guangzhou, China).

Vinyl silicone oils with a viscosity of 0.45 and 200 Pa s were adopted in system I and II, respectively. Tables 1 and 2 show the experimental formulation of the SRF for systems I and II, respectively.

2.2 Modeling and simulation details

The amorphous cell modules of the Materials Studio software 2020 were used to construct the molecular models including the molecular structures of different components during the SRF preparation (Fig. 1). The MD simulation modules constitute molecules a, b, c, d, e, and f corresponding to vinyl monofunctional silane (M) and tetrafunctional silane (Q) (MQ) silicone resin with a value M/Q ratio of 0.8, vinyl silicone oil with a viscosity of 10 Pa s, vinyl silicone oil with a viscosity of 0.45 Pa s, hydroxy silicone oil containing 5% hydroxyl, 1.6% hydrogen-containing silicone oil, and vinyl silicone oil with a viscosity of 200 Pa s, respectively.

The amorphous cell module was used to build the simulation box with molecules a, b, c, d, e, and f. Considering the limitation of the computer resources, the atomic number in a single molecular chain of systems was taken to be about 600–700. At the same time, the number of repeating units could not exceed 500. Therefore, it is crucial to choose the appropriate chain length of silicone rubber foam. According to Hildebrand's theory,[22] the solubility parameter of silicone rubber will tend to a constant value when the degree of polymerization of silicone rubber chains exceeded a certain critical value. Reducing the scale of the repeating units by 10 times met the above conditions. Therefore, the molecular chain of molecules b, c, and f was reduced in the same proportion during the simulation process, with a reduction ratio of 10. The repeat unit of molecules b, c, and f was 52, 18, and 364, respectively. The total number of atoms in the systems I and II was 4388 and 5136, respectively. The initial density was set to 1 g cm^{-3}. The reactive atoms on different chains were named R1 or R2 (as shown in the blue circle of Fig. 1). The cross-linked model was obtained by simulating the crosslinking process of groups R1 and R2, which were selected as the alternative crosslinks.

The force field parameters just like DREIDING and optimized potentials for liquid simulations (OPLS) will present some error at the simulation process except the temperature at 0 K.[23,24] The COMPASS force field is a high-performance and powerful force field, which can predict the microstructure, molecular conformation, and thermophysical properties of polymers within a wide range of temperature and pressure. The Forcite module was applied to optimize the molecular structure with COMPASS II as the force field.[25,26] During the geometric optimization process, the convergence thresholds for maximum energy change, maximum force, and maximum displacement were 0.001 kcal mol^{-1}, 0.5 kcal mol^{-1} $Å^{-1}$, and 0.015 Å, respectively. Then, 100 ps dynamic simulation was performed under the *NPT* ensemble (constant number of particles, pressure, and

Table 1 Experimental formulation of the SRF for system I

Component	Materials	Viscosity/Pa s	Vinyl content/%	Mole content/mol
A	Vinyl-terminated MQ silicone resin	100	1.3	0.00241
	Vinyl-terminated silicone oil	10	0.14	0.000691
	Vinyl-terminated silicone oil	0.45	0.4	0.00263
	Hydroxyl-terminated silicone oil	0.02	—	0.00471
B	Vinyl-terminated MQ silicone resin	100	1.3	0.00241
	Vinyl-terminated silicone oil	10	0.14	0.000691
	Vinyl-terminated silicone oil	0.45	0.4	0.00237
	Hydrogen-containing silicone oil	0.02	—	0.064

Table 2 Experimental formulation of the SRF for system II

Component	Materials	Viscosity/Pa s	Vinyl content/%	Mole content/mol
A	Vinyl-terminated MQ silicone resin	100	1.3	0.00241
	Vinyl-terminated silicone oil	10	0.14	0.000691
	Vinyl-terminated silicone oil	200	0.02	0.00132
	Hydroxyl-terminated silicone oil	0.02	—	0.00471
B	Vinyl-terminated MQ silicone resin	100	1.3	0.00241
	Vinyl-terminated silicone oil	10	0.14	0.000691
	Vinyl-terminated silicone oil	200	0.02	0.00119
	Hydrogen containing silicone oil	0.02	—	0.064

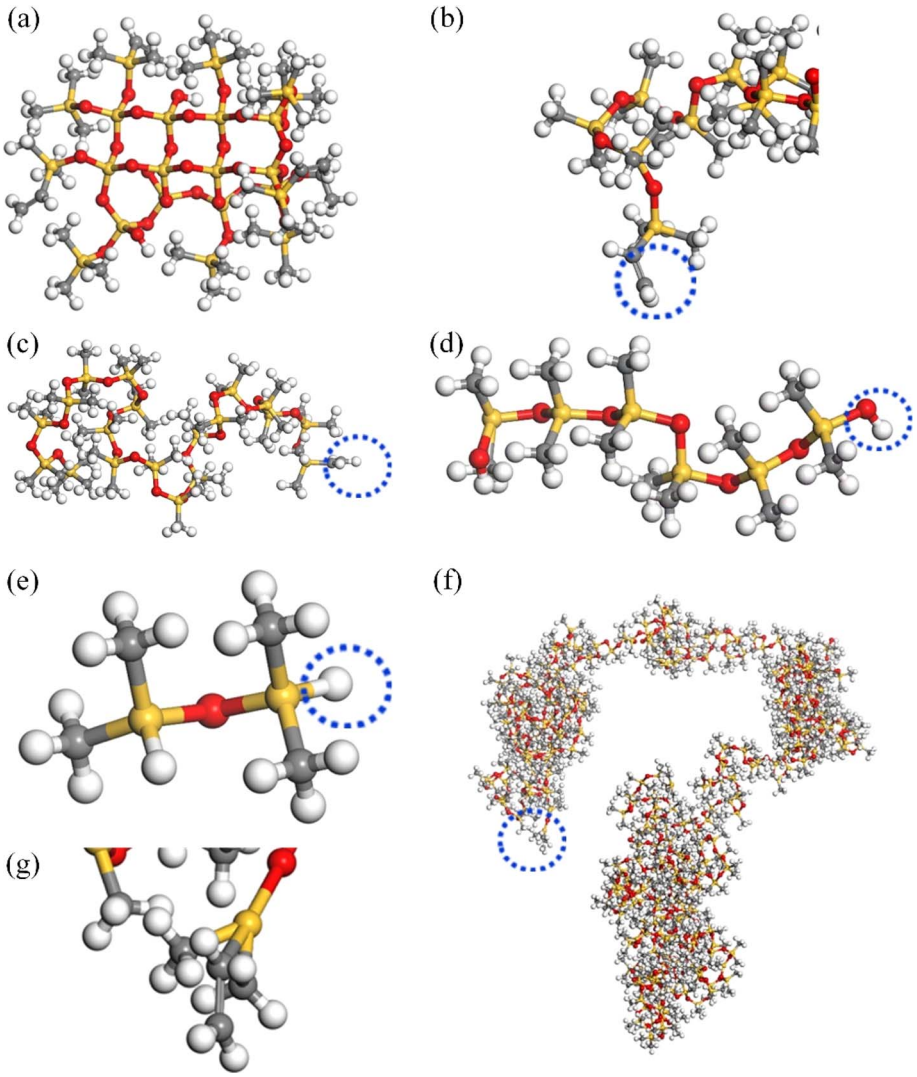

Fig. 1 SRF molecular structure. (a) Molecule a; (b) molecule b; (c) molecule c; (d) molecule d; (e) molecule e; (f) molecule f; and (g) the –CH=CH_2 of molecule f (gray: C, yellow: Si, red: O, and white: H).

temperature) at 0.0001 GPa and 298 K to determine the density fluctuations until the density–time curve was stable. To release the internal stress of the system, the model was annealed at 300–500 K, with a total of 200 000 steps. For further optimizing the structure, a 100 ps dynamic simulation was conducted under the *NPT* and *NVT* ensembles (constant number of particles, volume, and temperature), respectively. The precise Nose–Hoover temperature control mode and Berendsen pressure control mode were utilized in the dynamic process. The simulations were conducted at 298 K and a step size of 0.2 fs.

The energy curve of the optimized model is shown in Fig. 2. During the MD simulation of the SRF, the state of the entire

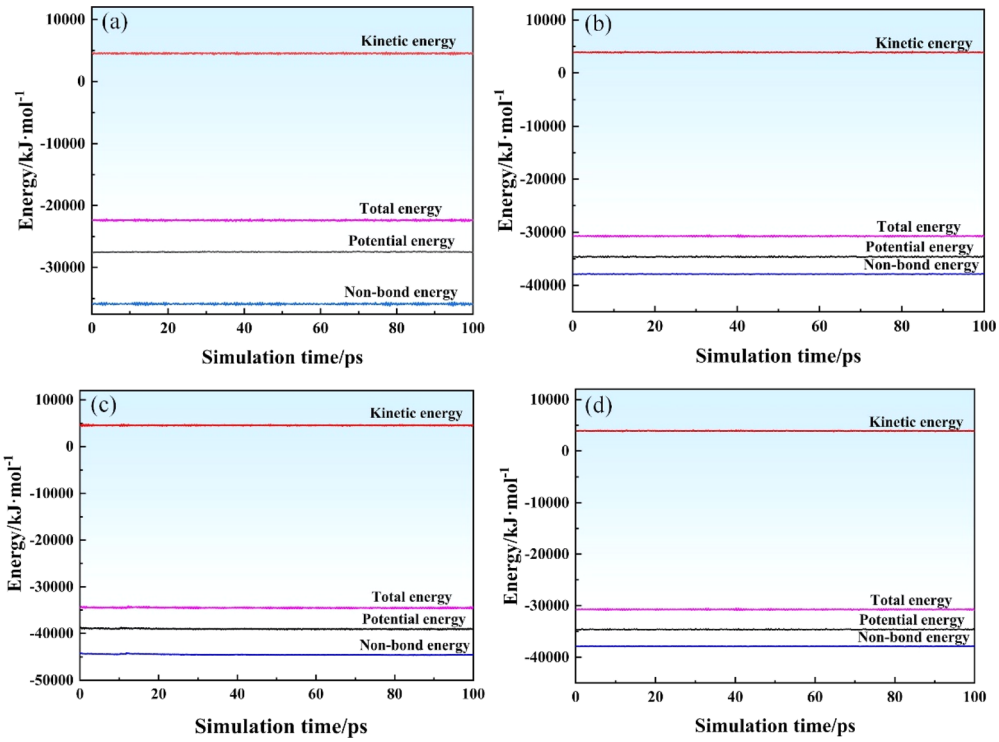

Fig. 2 Energy curve of the SRF *versus* simulation time. (a and b) *NPT* and *NVT* of system I; (c and d) *NPT* and *NVT* of system II.

simulation process must be meaningful and stable. The energy curves of these systems fluctuated in the range of ~1–5%, indicating the effectiveness of the simulation model. These results also confirmed that the two systems reached an equilibrium state.

2.3 Structure of the SRF before and after crosslinking

Fig. 3 shows the molecular structure of the SRF prepared using vinyl silicone oils of varying viscosities before and after crosslinking. The proportion of all components in the model for

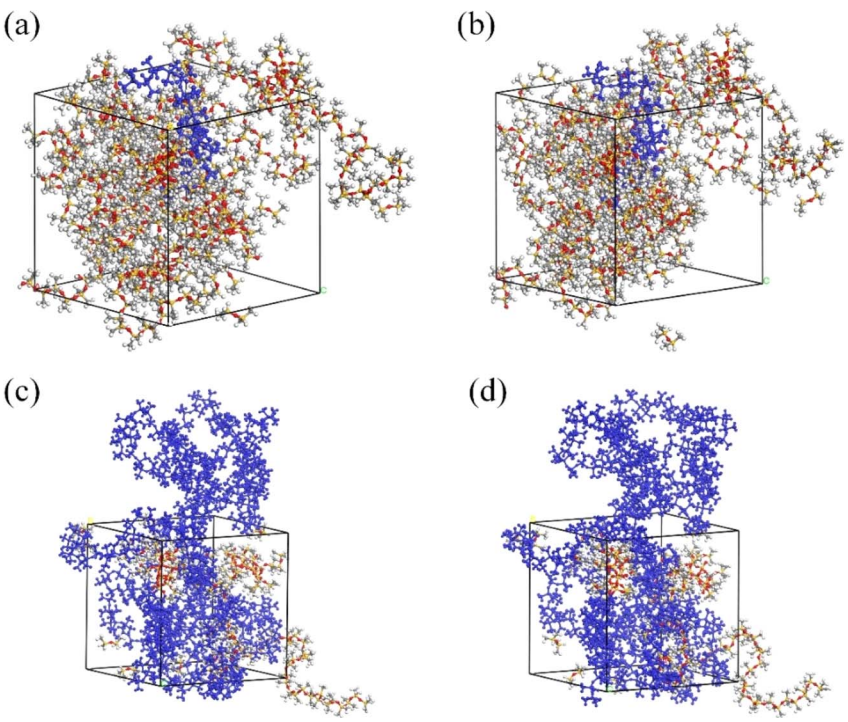

Fig. 3 Model diagram of the SRF before and after crosslinking. (a and b) Before and after crosslinking of system I; (c and d) before and after crosslinking of system II.

preparing the SRF also increased with an increase in the viscosity of vinyl silicone oil.

According to the research of Messinger,[27] it was found that the cellular microstructure had no effect on the mechanical properties of the organosiloxane foams. The mechanical properties were related to differences in molecular composition, structure, and polymer chain dynamics. This suggests that bubbles can be disregarded in simulations and that their presence does not invalidate the results. Therefore, it is reasonable to use molecular dynamic simulation without simulate bubbles in the simulation process for studying the SRF.

2.4 Preparation of the SRF and characterization

The SRF was prepared by vulcanizing components A and B at room temperature. The remaining components in both the systems were the same during the SRF preparation. Molecule e was chosen as the crosslinking agent. The Si–H group in the crosslinking agents underwent an addition reaction with the vinyl group in the molecules a, b, c, and f, forming new Si–C bonds. The Si–H group also condensed with the Si–OH group in molecule d to form Si–O–Si bonds and produce small molecules of hydrogen gas.[28]

Components A and B were stirred in a vacuum defoaming mixer (vacuum degree of −100 kPa) at 800 rpm. The flow chart for the SRF preparation is shown in Fig. 4. The two components were completely mixed in a 1 : 1 mass ratio and stirred for 2 min and quickly poured into a mold at room temperature. Then, the molding plate was cured at 60 °C and post-cured at 150 °C for 15 min, yielding the SRF. Post-curing improved the degree of curing and the components reacted completely at 150 °C, which improved the mechanical properties of the SRF and eliminated any volatile substances.

There has two main methods for analyzing the mechanical properties of system, static and dynamic method in MD simulation, respectively. In the static method, the bond angle was fixed, whereas the influence of configuration entropy on the elastic constant was disregard. Contrarily, the dynamic method is time-consuming and suffers from uncertainties in the results due to strain fluctuations. Therefore, the static method was used for simulation herein.

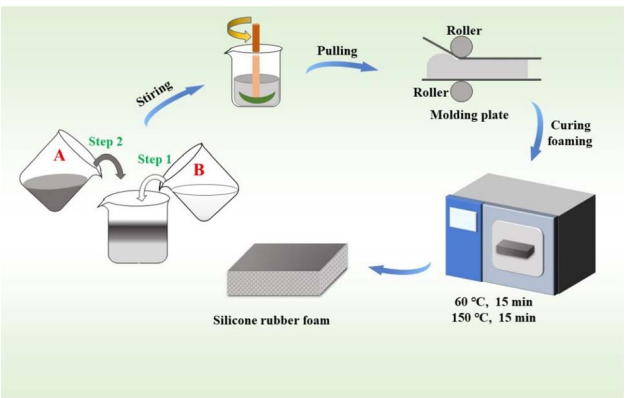

Fig. 4 Flow chart for the SRF preparation.

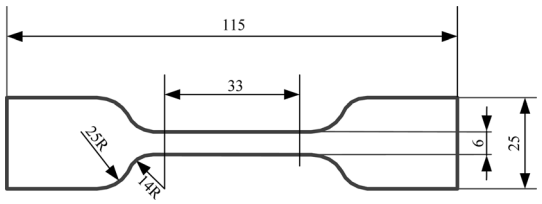

Fig. 5 Schematic of the dumbbell sample.

The static mechanical properties of the SRF were measured using an electronic universal testing machine (E43.104, MTS) and an axial extensometer (ZEM5.204, ZHIXIN). A schematic of the dumbbell sample is shown in Fig. 5. The effective part of the sample was 33 mm × 6 mm × 5 mm (length × width × thickness). During the experiment, the sample was uniformly stretched with a stretching rate of 50 mm min^{-1}. For each set of data on the materials' properties, at least five samples were tested for each system and the values were averaged.

The VTMR12-010V-I nuclear magnetic resonance (NMR) crosslinking densimeter was used to test the crosslinking density of the foaming materials. The effective detection range of the sample was $\varphi 8.5 \times H20$ mm. The magnetic field intensity was set to 0.5 ± 0.05 T. The crosslinking density was determined at 30 °C. LX-C shore hardness testers were utilized to measure the shore hardness (shore C) of the SRF. The tensile strength and elongation at break of the SRF were tested using the WDW-10 universal testing machine at a tensile rate of 500 mm min^{-1}. The sample was stretched uniformly during the experiment. Five samples were measured, and the average value was used as the final value in the experiment.

3. Results and discussion

3.1 Motion of molecular chains

3.1.1 Mean square displacement. The mean square displacement (MSD) can effectively reflect the mobility of polymer chains,[29] which is an important index of polymer materials. The motion of polymer chains considerably impacts on the mechanical properties of polymer materials.[30] MSD is calculated as follows:[20,31]

$$\mathrm{MSD} = \langle |r_i(t) - r_i(0)|^2 \rangle \quad (1)$$

where $r_i(t)$ and $r_i(0)$ are the position vectors of the atom i at time t and 0, respectively. The brackets $\langle\ \rangle$ denote for the average square of the displacement.

Fig. 6 shows the MSD curves of molecular chains of different components in the two systems at 298 K. A linear correlation existed between the MSD and the simulation time, indicating that the diffusion system was in a state of normal diffusion. MSD curve showed an upward trend as the simulation time increased. Fig. 6(a) and (b) show that the MSD of system II is smaller than that of system I. To accurately analyze the MSD curves, the MSDs of functional groups in the system were determined (Table 3). The MSD of the Si–H bond was the highest, whereas those of –CH=CH_2 in molecules c and f is

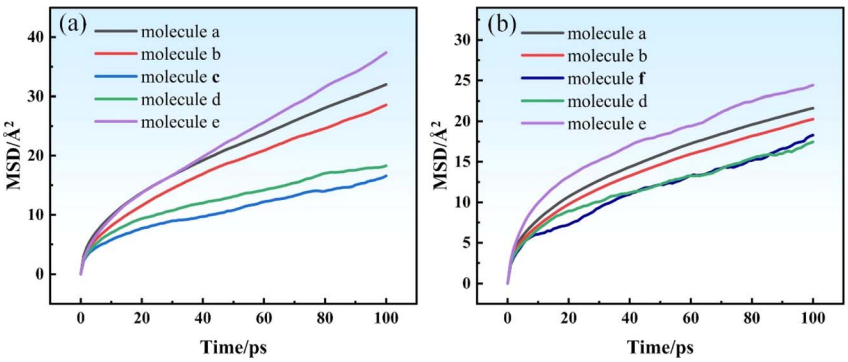

Fig. 6 MSD curves for various systems, (a) system I; (b) system II.

Table 3 MSD of the SRF in two systems I and II

	MSD/Å²	
Component	System I	System II
Si–O–Si (silicon resin)	31.99	21.62
–CH=CH$_2$ (vinyl silicone oil of 0.45 Pa s)	16.6	—
–CH=CH$_2$ (vinyl silicone oil of 10 Pa s)	28.59	20.26
–CH=CH$_2$ (vinyl silicone oil of 200 Pa s)	—	18.30
Si–H (hydrogen containing silicone oil)	37.39	24.43
Si–OH (hydroxy silicone oil)	18.37	17.45

Table 4 D value of the SRF in systems I and II

	D/(Å² ps^{-1})	
Component	System I	System II
Si–O–Si (molecule a)	0.0352	0.0189
–CH=CH$_2$ (molecule b)	0.0314	0.0184
–CH=CH$_2$ (molecule c)	0.0173	—
Si–OH (molecule d)	0.0182	0.0168
Si–H (molecule e)	0.0477	0.0215
–CH=CH$_2$ (molecule f)	—	0.0196

relatively smaller, primarily because hydrogen-containing silicone oil has shorter molecular chains. Thus, the molecules can easily move, which results in a larger MSD. Contrarily, vinyl silicone oil has longer molecular chains, which cannot move easily, resulting in a smaller MSD. Moreover, system I has a shorter molecular chain and a larger free volume than system II, which facilitates easier molecular chain movement. A shorter molecular chain length implies that the resistance of motion in the system is lower, and the MSD of the molecular chain is the larger.

3.1.2 Diffusion coefficient. The diffusion coefficient (D) is one of the essential parameters in determining the mobility of polymer chains. The D is selected the linear part of the MSD curve for each component of the SRF.[32] The D can be obtained as follows:[33]

$$D = \lim_{t\to\infty}\frac{1}{6t}\left\langle |r_i(t) - r_i(0)|^2 \right\rangle = \frac{\mathrm{MSD}}{6t} \quad (2)$$

where $r_i(t)$ and $r_i(0)$ are the position vector of the atom i at time t and 0, respectively. MSD is mean square displacement. The brackets $\langle\ \rangle$ denote for the average square of the displacement.

Table 4 shows the D of the SRF in systems I and II. It can be seen that system I had a larger D. This is due to the 0.45 Pa s vinyl silicone oil has short molecular chains, relatively small molecular weight, and large free volume within the system, allowing easy molecular chains movement.

3.1.3 Fractional free volume. The fractional free volume (FFV) of a polymer is defined as the ratio of the free volume to the total volume of the polymer composite.[34] The free volume is obtained by subtracting the occupied volume of molecular chains from the total volume of polymer materials. It provides space for the movement of polymer molecular chains. Generally, as the free volume decreases, the molecular motion of polymer materials becomes more difficult. The FFV is calculated as follows:[35]

$$\mathrm{FFV} = 1 - \frac{V_0}{V} \quad (3)$$

where V_0 denotes the occupied volume and V denotes the total volume of a polymer.

Fig. 7 shows the free volume morphology of the SRF with different vinyl silicone oil viscosities. The free and occupied volume of the SRF are denoted in blue and gray, respectively. The FFV of the SRF with different viscosities of vinyl silicone oil is shown in Table 5. Fig. 7 and Table 5 show that the free volume and FFV decrease as of vinyl silicone oil viscosity increases. This is due to the 200 Pa s vinyl silicone oil has a long molecular chain, relatively large molecular weight, larger volume of polymer chains, and smaller FFV. A larger FFV allows for more active movement of molecules within a larger space, thereby increasing the diffusion coefficient.[36] This finding is consistent with the previous results of MSD and D values.

3.1.4 Binding energy. Binding energy (E_{binding}) is defined as the negative value of the intermolecular interaction energy (E_{inter}).[37] E_{binding} reflects the energy consumed to overcome the intermolecular attraction for separating all the molecules in

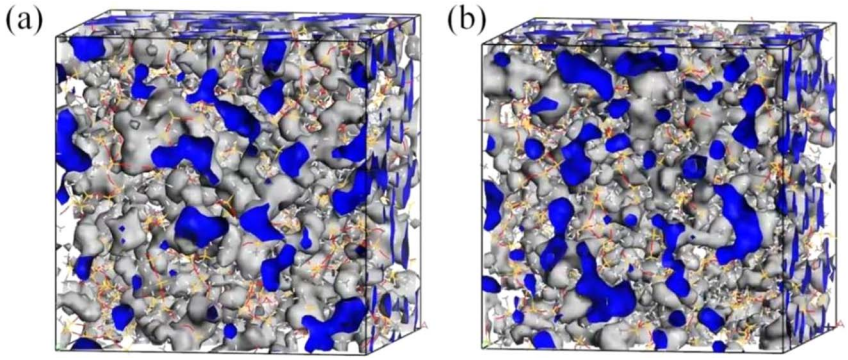

Fig. 7 Free volume morphology of the SRF with different vinyl silicone oil viscosities. The blue denotes the area of free volume. (a) System I; (b) System II.

Table 5 FFVs of the SRF with different viscosities of vinyl silicone oil

Systems	System I	System II
Free volume/A^3	11 252.53	13 069.62
Occupied volume/A^3	41 551.33	48 563.77
FFV/%	21.31	21.21

a system to infinity. $E_{binding}$ can also reflect the compatibility between the components of a system. In general, a higher the $E_{binding}$ indicates a stronger the attraction between the system components, better system compatibility, and a more stable the blend system. The $E_{binding}$ is calculated as follows:[38,39]

$$E_{binding} = -E_{inter} = -(E_{total} - E_{-CH=CH_2} - E_{Si-OH} - E_{Si-H}) \quad (4)$$

where E_{inter}, E_{total}, E_{Si-OH}, and E_{Si-H} are the interaction energy, total system energy, free energy of molecular d, and free energy of molecule e, respectively. $E_{-CH=CH_2}$ is the free energy of molecules a, b, c, and f, respectively.

Tables 6 and 7 show the free energies of different components and the $E_{binding}$ of systems I and II. After simulation, the $E_{binding}$ of the SRF prepared using vinyl silicone oils of 0.45 and 200 Pa s were 551.52 and −604.30 kcal mol^{-1}, respectively. The absolute value of the $E_{binding}$ in system II was slightly higher than that in system I, with a difference of ∼52.78 kcal mol^{-1}. Based on the sign of the $E_{binding}$, the compatibility of two components of the SRF can be confirmed.[39] A negative $E_{binding}$ indicates that the components have a poor compatibility, and a positive $E_{binding}$ indicates their good compatibility. A larger positive $E_{binding}$ implies the components of the two systems will have better compatibility.[40] The stability of the SRF is affected by the magnitude of $E_{binding}$. A larger absolute value of the $E_{binding}$ will enhance the system stability.[41] Moreover, the $E_{binding}$ is influenced by the molecular chain length. System I has better compatibility for the two components due to the positive $E_{binding}$ and shorter molecular chains; therefore, the molecules are compatible with each other in this system.

Table 6 Free energies of different components in systems I and II

	Free energy/(kcal mol^{-1})	
Functional group/item	System I	System II
E_{total}	−34 545.413	−36 946.094
Si–O–Si (E_a)	−11 581.263	−4884.269
–CH=CH$_2$ (10 Pa s) (E_b)	−8343.170	−3381.280
–CH=CH$_2$ (0.45 Pa s) (E_c)	−7727.943	—
–CH=CH$_2$ (200 Pa s) (E_f)	—	−986.613
Si–OH (E_d)	−2344.130	−1693.140
Si–H (E_e)	−3997.385	−26 605.088

Table 7 $E_{binding}$ of systems I and II

Item	$E_{binding}$/kcal mol^{-1}
System I	551.52
System II	−604.30

3.1.5 Cohesive energy density and solubility parameter. The cohesive energy density (CED) is the energy required per unit mole of a polymer transitioning from liquid to gas in per unit volume.[42,43] The CED is also a physical quantity for describing the magnitude of intermolecular forces and can be utilized as a criterion for evaluating the material stability. The CED of polymers can be determined *via* MD simulations without damaging their molecular structure. The CED of the SRF can be calculated as follows:[44]

$$CED = \frac{E_{cohesive}}{V} = \frac{E_{inter}}{V} \quad (5)$$

where $E_{cohesive}$ is the cohesive energy of the system, V is the volume of the system, and E_{inter} is the total intermolecular energy of the system.

The solubility parameter (δ) is applied to determine the compatibility and dissolution characteristics of different components or polymers. It is the square root of the CED and can be determined for the SRF as follows:[40]

$$\delta = \sqrt{CED} \quad (6)$$

where δ is the solubility parameter and CED is the cohesive energy density.

Table 8 shows that the CED and δ of the SRF prepared using vinyl silicone oils of 0.45 and 200 Pa s are 1.717 × 10^8 J m^{-3} and

Table 8 CED and δ of the SRF in systems I and II

Item	CED/(J m^{-3})	δ/(J cm^{-3})$^{1/2}$
System I	1.717×10^8	13.104
System II	1.540×10^8	12.408

13.104 (J cm^{-3})$^{1/2}$ as well as 1.540×10^8 J m^{-3} and 12.408 (J cm^{-3})$^{1/2}$, respectively. As the viscosity of the vinyl silicone oil increases, the CED and δ of the SRF decrease, indicating weak interaction between the SRF components. The higher the CED and δ, the better the compatibility between the components in the SRF. Thus, system I has better compatibility than system II. This finding is consistent with the $E_{binding}$ results.

Moreover, δ decreases with increasing viscosity of vinyl silicone oil and the number of repeating units. This result is consistent with that reported previously,[40] where the δ of NR and SBR gradually decreased as the number of N_{unit} (chain repeating units) increased.

3.1.6 Radial distribution function. The radial distribution function (RDF) is the probability of finding other atoms at a distance r from the central atom.[45,46] It can also reflect the characteristics of material microstructures and reveal the properties of interactions between nonbonded atoms. The RDF is calculated as follows:[47,48]

$$g_{C-D}(r) = \frac{n_D V}{4\pi r^2 dr N_D} \quad (7)$$

where n_D is the number of D atoms surrounding atom C at a distance r, N_D is the total number of D atoms, and V is the volume of the whole system. Atom C is the Si–H bond in molecule e. Atom D is –CH=CH$_2$ of molecules a, b, c, and f, and Si–OH in molecule d.

Fig. 8 shows the RDFs of the SRF for the vinyl silicone oil viscosities of 0.45 and 200 Pa s, respectively. The RDFs of other atoms (such as Si–OH and –CH=CH$_2$) found around the Si–H in hydrogen-containing silicone oil as the central atom has a significant peak at a certain distance. This indicates that Si–H has a strong attraction to other atoms around this distance. Moreover, the RDFs of the five components in the SRF are similar in the number, distribution, and patterns of peaks, but the peak values are different.

As vinyl silicone oil viscosity increases, the SRF forms looser aggregates and a relatively large $g(r)$ peak is observed. As shown in Fig. 8(a), the maximum $g(r)$ of molecules a, b, c, and d are 0.96, 1.51, 1.40, and 1.48, respectively. These peaks are observed at positions of 5.37, 5.53, 5.09, and 7.49 Å from the Si–H bond, respectively. As shown in Fig. 8(b), the maximum $g(r)$ of molecules a, b, f, and d are found to be 1.78, 1.16, 2.46, and 0.89, respectively. These peaks are observed at positions of 5.01, 9.69, 5.85, and 7.45 Å from the Si–H bond, respectively. Overall, the RDF of system I is smaller than that of system II. The shorter the molecular chain of system I, the higher the vinyl content, and the tighter the molecular configuration of the SRF after cross-linking. The $g(r)$ peak values of the components in the system I are relatively low, the aggregation of molecular chains is stronger, and the distribution of system components is more uniform. These results are consistent with the solubility parameters and $E_{binding}$ results.

3.1.7 Radius of gyration. The radius of gyration (R_g) is one of the parameters for describing the three-dimensional configuration of a molecule. It is the distance between the molecular center of mass and the atom farthest from that center of mass. R_g can also be used to measure the compactness and molecular aggregation of the SRF.[49] A larger R_g implies a smaller aggregation degree of the molecular chain. A lower R_g indicates that the molecular structure of the SRF is more aggregated or closely packed. If the structure of the polymer is highly stable, R_g will also be relatively stable. It is determined as follows:[50,51]

$$R_g = \sqrt{\frac{\sum_{n}^{i=1} m_i r_i^2}{\sum_{n}^{i=1} m_i}} \quad (8)$$

where R_g is the radius of rotation of the molecular chain; n is the number of atoms in the molecular chain; m_i is the atomic mass, and r_i is the distance from the atom to the centroid of the molecular chain.

Fig. 9 shows the R_g of the SRF at different vinyl silicone oil viscosities. The R_g value is 12 and 31 Å at viscosities of 0.45 and 200 Pa s, respectively. The structure of system II has a lower aggregation degree. The reason is that vinyl silicone oil has a higher molecular weight and lower vinyl content; therefore, it

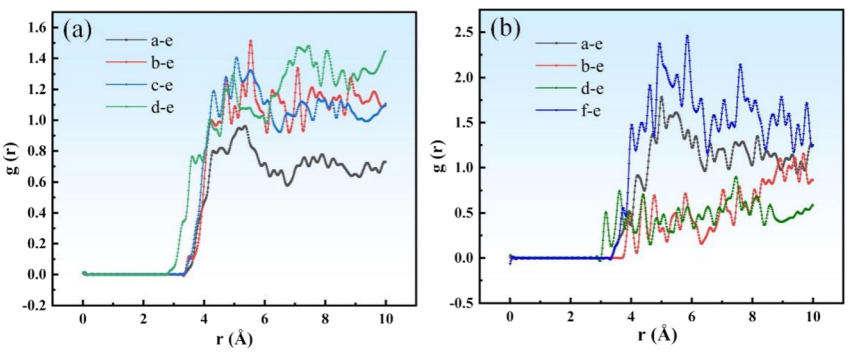

Fig. 8 Total $g(r)$ of Si–H for different viscosities of vinyl silicone oils; the plots on the left and right represent different distances (r). (a) System I; (b) System II.

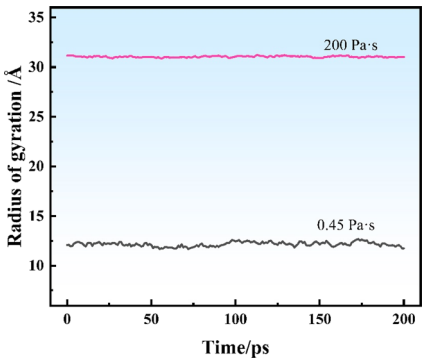

Fig. 9 R_g of 200 ps for various viscosities of vinyl silicone oil.

forms fewer new chemical bonds. This finding is consistent with the RDF results, indicating that the peak value of the RDF is higher in system II.

An increase or decrease in R_g implies disaggregation or aggregation between the molecules, respectively.[52] If the molecular aggregates are stable, R_g will be relatively stable. Contrarily, if the molecular aggregates undergo rearrangement or rebonding during the MD simulation, R_g values change over time. Fig. 9 shows R_g values of systems I and II are stable, indicating that the structure did not undergo significant expansion or contraction of during the crosslinking process and confirming its stability during the simulation of components.

3.2 Static mechanical properties

Mechanical properties are an essential basic property related to the preparation and application of the SRF.[53–55] The static mechanical properties of the SRF after crosslinking were calculated *via* MD simulation at 298 K. The mechanical properties of the models were calculated using the constant-strain energy minimisation method. Molecular dynamic simulations allowed stress and strain analysis of systems under small deformation. By applying a micro strain to a system that has reached equilibrium, the stress–strain relationship follows Hooke's law, and the elastic stiffness tensor can be expressed as follows:[56]

$$\sigma_i = C_{ij}\varepsilon_j \tag{9}$$

where σ_i represents the stress tensor element, ε_j represents the corresponding symmetric strain tensor element, and C_{ij} is stiffness matrix.

The stiffness matrix C_{ij} can be obtained from eqn (9) as follows:[57,58]

$$C_{ij} = \begin{bmatrix} \lambda+2\mu & \lambda & \lambda & 0 & 0 & 0 \\ \lambda & \lambda+2\mu & \lambda & 0 & 0 & 0 \\ \lambda & \lambda & \lambda+2\mu & 0 & 0 & 0 \\ 0 & 0 & 0 & \mu & 0 & 0 \\ 0 & 0 & 0 & 0 & \mu & 0 \\ 0 & 0 & 0 & 0 & 0 & \mu \end{bmatrix} \tag{10}$$

where λ and μ are the elastic constants.

The elastic constants can be calculated from the stiffness matrix as follows:

$$\lambda = \tfrac{1}{6}(C_{12} + C_{13} + C_{21} + C_{23} + C_{31} + C_{32}) \tag{11}$$

$$\mu = \tfrac{1}{3}(C_{44} + C_{55} + C_{66}) \tag{12}$$

The mechanical properties parameters such as elastic modulus (E), shear modulus (G), bulk modulus (B), and Poisson's ratio (ν) of the system are determined as follows:[59–61]

$$E = \frac{\mu(3\lambda+2\mu)}{(\lambda+\mu)} \tag{13}$$

$$G = \mu \tag{14}$$

$$B = \lambda + 2\mu/3 \tag{15}$$

$$\nu = \frac{\lambda}{2(\lambda+\mu)} \tag{16}$$

Table 9 shows the experimental and simulation results of static mechanical properties in systems I and II, with some errors. The values of parameters determined *via* MD simulations were slightly higher. The errors between the experimental and simulation values were related to the molecular chain length of the polymers. The degree of polymerization of molecules b, c, and f was reduced in the same proportion during the simulation process. The molecules repeat units simulated by molecular dynamics is about 10 times shorter than that of the molecules in the experiment. A shorter the molecular chain implies a higher the vinyl content, and a tighter the molecular configuration of the SRF after crosslinking, leading to higher mechanical properties of the SRF. Thus, the reduction in molecular chain length is the main reason for the higher simulation results of the SRF.

The changes in the mechanical properties of the SRF with the increasing of the vinyl silicone oil viscosity determined *via* MD simulation were consistent with those determined experimentally. A comparison of the SRF in systems I and II shows

Table 9 Experimental and simulation results of the static mechanical properties of systems I and II

	Experimental results				Simulation results			
Item	E/MPa	G/MPa	B/MPa	ν	E/GPa	G/GPa	B/GPa	ν
System I	2.450	2.694	2.811	0.366	0.7217	0.9512	0.6452	0.4592
System II	0.997	1.370	0.663	0.247	0.6422	0.2920	0.3575	0.4279

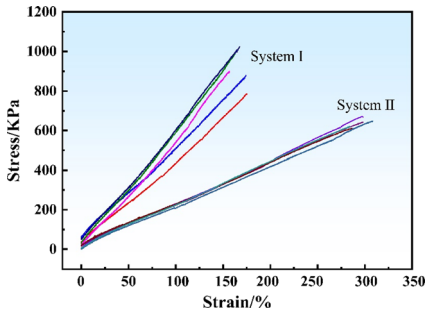

Fig. 10 Stress–strain curves of the SRF in systems I and II.

that the static mechanical properties of system II decrease. As the viscosity of vinyl silicone oil increases, the elastic modulus, shear modulus, bulk modulus, and Poisson's ratio of the SRF decrease to ~59.3%, 49.1%, 76.4%, and 32.5%, respectively, as determined experimentally. These values were determined *via* MD simulation as ~11.0%, 69.3%, 44.6% and 6.8%, respectively.

Fig. 10 shows the stress–strain curves of the SRF in systems I and II. The slope value of the elastic stage in the stress–strain curve represents the elastic modulus of each system. System I had a relatively large slope, indicating its higher elastic modulus than system II. This finding is consistent with the results shown in Table 9. These results indicated that changing the vinyl silicone oil viscosity considerably impacted on static mechanical properties of the SRF.

Fig. 11(a)–(d) show the crosslinking density, shore C, tensile strength, and elongation at break of the SRF in systems I and II, respectively. The crosslinking density of the SRF decreases from 4.62 to 4.07 mol mL^{-1}, and shore C decreases from 44.5° to 29°. The tensile strength decreases from 0.86 to 0.61 MPa, whereas the elongation at break increases from 83.4% to 153.5%. As the viscosity of vinyl silicone oil increases, the crosslinking density, shore C, and tensile strength of the SRF decrease, whereas the elongation at break increases. As the viscosity of vinyl silicone oil increases, the length of polymer molecular chains increases and the vinyl content decreases, which loosens the cross-linked network structure of the SRF. The network structure tightens when the vinyl content is high. This indicates that the viscosity of vinyl silicone oil can influence the structure and properties of the SRF. Vinyl silicone oil with a lower viscosity can enhance the crosslinking density of silicone rubber, thereby increasing its tensile strength and hardness. In contrast, vinyl silicone oil with a higher viscosity can impart greater elasticity and longer elongation to silicone rubber. These results were also reported in a previous study.[62] Thus, by selecting an appropriate the viscosity of vinyl silicone oil, the SRF with a desired structure and performance can be prepared.

The performance of the SRF cannot be determined solely based on one parameter. For instance, a larger MSD of the system does not necessarily indicate poor performance. A comprehensive analysis must be conducted by considering various parameters such as RDF and δ as well as the application prospects. The cross-linked network structure of the SRF considerably affects the mechanical properties of the SRF. Additionally, the application and requirements of the SRF, such as sealing or cushioning and shock absorption, must be considered to determine its performance.

However, the effect of high-viscosity vinyl silicone oil on the movement of molecular chains and the aggregation degree of molecular structure of the SRF needs futher elucidation. To this end, we noted the following observations. (1) A longer molecular chain implies smaller free volume of the system, the weaker activity of the system's molecular chain, and the lower MSD. (2)

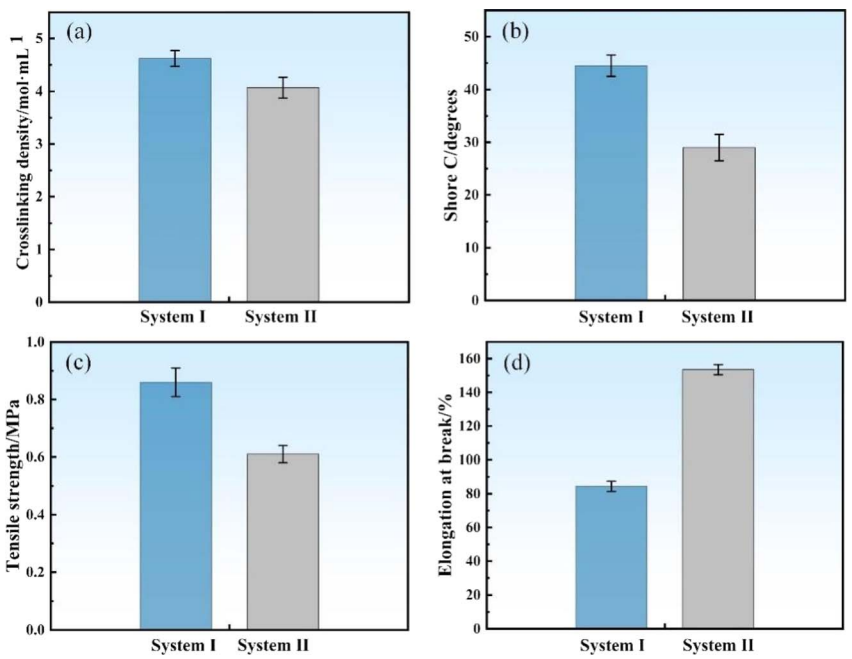

Fig. 11 Mechanical properties of SRF in systems I and II. (a) Crosslinking density; (b) shore C; (c) tensile strength; (d) elongation at break.

System II has a negative $E_{binding}$ and lower CED and δ; therefore, its components have poor compatibility. (3) The low vinyl content in the system, fewer crosslinking agents, and low-density network structure increases the R_g. (4) The RDF shows that the aggregation degree of molecular structure in system II is relatively low. Thus, the mechanical property of the SRF is affected by the ability of molecular motion, the size of free volume, multicomponent compatibility, binding energy of the whole system, and the aggregation degree of its molecular chain structure. The mechanical properties of the SRF can be optimized based on the aforementioned parameters.

4. Conclusions

Herein, MD simulation was performed on the molecular motion trajectories of the SRF prepared using vinyl silicone oil of varying viscosities from the perspective of all atomic molecules using Materials Studio. Moreover, the simulation and experimental results were analyzed and compared. The following main conclusions were drawn:

(1) The polymer molecular chain length is crucial for the SRF performance. As the viscosity of vinyl silicone oil increases, the MSD of the system decreases and $E_{binding}$ increases. Meanwhile, the CED and the solubility parameter decrease, leading to poor compatibility between the system components. The aggregation degree weakens with increasing R_g. Thus, the mechanical properties of the system are influenced by the viscosity of vinyl silicone oil.

(2) As the viscosity of vinyl silicone oil increases, the vinyl content decreases, and fewer network structures are formed within the system. The elastic modulus, shear modulus, bulk modulus, and Poisson's ratio of the SRF decrease. The crosslinking density, shore C, and tensile strength of the SRF also decrease, whereas the elongation at break increases. Thus, by selecting an appropriate the viscosity of vinyl silicone oil, the desired performance of SRF can be obtained.

(3) Although some minor differences were observed between the MD simulation and experiment results, they were largely consistent. This provides theoretical support and reference value for the industrial production of the SRF from a microscopic perspective.

Data availability

Data will be made available on request.

Authors contribution

Hongyu He: conceptualization, data curation, investigation, methodology, software, visualization, writing – original draft. Lulu Li: conceptualization, data curation, writing – review & editing. Ruhan Ya: conceptualization, writing – review & editing. Hong Liu: upervision, methodology. Bin Luo: methodology, funding acquisition. Zhipeng Li: methodology, formal analysis, resources, writing – review & editing, supervision. Wenhuai Tian: conceptualization, funding acquisition, investigation, writing – review & editing.

Conflicts of interest

The authors declare that they have no known competing financial interests or personal relationships that could have appeared to influence the work reported in this paper.

Acknowledgements

The computing work is supported by USTB MatCom of Beijing Advanced Innovation Center for Materials Genome Engineering. This work was financially supported by Foshan Science and Technology Innovation Special Fund Project (No. BK21BE009 and BK22BE004).

References

1 M. Tripathi, S. Parthasarathy, R. Yadav and P. K. Roy, Flexible Silicone-Hollow Glass Microballoon Syntactic Foams for Application in Fire Protective Clothing, *J. Appl. Polym. Sci.*, 2022, **139**(19), e52101.
2 Y. X. Han, L. J. Yang, Z. Yu, Y. J. Zhao and Z. X. Zhang, Lightweight and Flame Retardant Silicone Rubber Foam Prepared by Supercritical Nitrogen: The Influence of Flame Retardants Combined with Ceramicizable Fillers, *Constr. Build. Mater.*, 2023, **370**(17), 130735.
3 A. M. Golobic, T. M. Bryson, T. H. Weisgraber, J. A. Armas, E. B. Duoss, T. S. Wilson and J. M. Lenhardt, Controlled in Situ Foaming for Mechanical Responsiveness of Architected Foams, *Adv. Eng. Mater.*, 2023, **25**(23), 2301335.
4 A. H. Landrock, *Handbook of Plastic Foams: Types, Properties, Manufacture and Applications*, Noes Publications, Park Ridge, 1995.
5 C. F. Cao, P. H. Wang, J. W. Zhang, K. Y. Guo, Y. Li, Q. Q. Xia, G. D. Zhang, L. Zhao, H. Chen, L. B. Wang, J. F. Gao, P. A. Song and L. C. Tang, One-Step and Green Synthesis of Lightweight, Mechanically Flexible and Flame-Retardant Polydimethylsiloxane Foam Nanocomposites via Surface Assembling Ultralow Content of Graphene Derivative, *Chem. Eng. J.*, 2020, **393**, 124724.
6 N. Boumdouha, J. Duchet-Rumeau and J. F. Gerard, Structure Property and Performance of Polymeric Foams: A Review, *J. Basic Appl. Sci.*, 2024, 201–222.
7 H. W. Pan, C. G. Zang and Y. L. Zhang, Effect of Vinyl-Terminated Silicone Oil Chain Length and Reinforcing Agent on the Properties of Silicone Rubber, *Key Eng. Mater.*, 2022, **905**, 221–230.
8 S. A. Hollingsworth and R. O. Dror, Molecular Dynamics Simulation for All, *Neuron*, 2018, **99**(6), 1129–1143.
9 M. H. N. Pour, G. Payganeh and M. Tajdari, Experimental and Numerical Study on the Mechanical Behavior of 3D Printed Re-entrant Auxetic Structure Filled with Carbon Nanotubes-Reinforced Polymethylmethacrylate Foam, *Mater. Today Commun.*, 2023, **34**, 104936.
10 A. Vasilev, T. Lorenz and C. Breitkopf, Prediction of Thermal Conductivities of Rubbers by MD Simulations-New Insights, *Polymers*, 2022, **14**(10), 2046.

11 S. Pahari, P. Ghosh and R. Mukhopadhyay, Prediction of Thermodynamic and Viscoelastic Properties of Rubber Using Molecular Simulations, *SAE Technical Paper*, 2023, No. 2023-28-1312.
12 K. Lee, Y. L. Sim, H. Jeong, A. Kim, Y. Lee, S. E. Shim and Y. J. Qian, Mechanochemically Functionalized and Fibrillated Microcrystalline Cellulose as a Filler in Silicone Foam: an Integrated Experimental and Simulation Investigation, *Carbohydr. Polym.*, 2024, **327**, 121660.
13 Q. H. Wei, Y. E. Wang, W. H. Chai, T. Wang and Y. F. Zhang, Effects of Composition Ratio on the Properties of Poly(Vinyl Alcohol)/Poly (Acrylic Acid) Blend Membrane: a Molecular Dynamics Simulation Study, *Mater. Des.*, 2016, **89**, 848–855.
14 L. Zhu, S. G. Zhao, C. Zhang, X. Cheng, J. H. Hao, X. Q. Shao and C. J. Zhou, Effects of Chain Structure on Damping Property and Local Dynamics of Phenyl Silicone Rubber: Insights from Experiment and Molecular Simulation, *Polym. Test.*, 2021, **93**, 106885.
15 K. L. S. Yip and S. John, Sound Trapping and Waveguiding in Locally Resonant Viscoelastic Phononic Crystals, *Sci. Rep.*, 2023, **13**(1), 15313.
16 A. ReghunadhanH. AkhinaA. R. AjithaN. ChandranS. T. Nair H. J. MariaS. ThomasThermoplastic Elastomers (TPEs) from Rubber-Plastic Blends, *Advances in Thermoplastic Elastomers*, 2024, pp. 291–314.
17 D. Kruszewski, R. B. Malla and M. T. Shaw, Bonding and Aging Behavior of Silicone Foam Sealant for Small Movement Bridge Joints, *Int. J. Civ. Eng.*, 2023, **21**(2), 205–217.
18 E. Rostami-Tapeh-Esmaeil and D. Rodrigue, Morphological, Mechanical and Thermal Properties of Rubber Foams: a Review Based on Recent Investigations, *Materials*, 2023, **16**(5), 1934.
19 S. Marl, M. Hartung, K. Klier, A. Rüppel, R. U. Giesen and H. P. Heim, Improvement of the Cell Structure of Water-Foamed Liquid Silicone Rubber, *Adv. Eng. Mater.*, 2023, 2201898.
20 W. T. Lou, C. Y. Xie and X. F. Guan, Molecular Dynamic Study of Radiation-Moisture Aging Effects on the Interface Properties of Nano-Silica/Silicone Rubber Composites, *npj Mater. Degrad.*, 2023, **7**(1), 32.
21 X. Li, J. Liu and Z. J. Zheng, Recent Progress of Elastomer-Silica Nanocomposites toward Green Tires: Simulation and Experiment, *Polym. Int.*, 2023, **72**(9), 764–782.
22 M. Belmares, M. Blanco, W. A. Goddard III, R. B. Ross, G. Caldwell, S. H. Chou, J. Pham, P. M. Olofson and C. Thomas, Hildebrand and Hansen solubility Parameters from Molecular Dynamics with Applications to Electronic Nose Polymer Sensors, *J. Comput. Chem.*, 2004, **25**(15), 1814–1826.
23 S. L. Mayo, B. D. Olafson and W. A. Goddard, DREIDING: a Generic Force Field for Molecular Simulations, *J. Phys. Chem.*, 1990, **94**(26), 8897–8909.
24 W. L. Jorgensen and J. Tirado-Rives, The OPLS Force Field for Proteins. Energy Minimizations for Crystals of Cyclic Peptides and Crambin, *J. Am. Chem. Soc.*, 1988, **110**(6), 1657–1666.
25 N. D. Kondratyuk and V. V. Pisarev, Calculation of Viscosities of Branched Alkanes from 0.1 to 1000 MPa by Molecular Dynamics Methods Using COMPASS Force Field, *Fluid Phase Equilib.*, 2019, **498**, 151–159.
26 H. Sun, P. Y. Ren and J. R. Fried, The COMPASS Force Field: Parameterization and Validation for Phosphazenes, *Comput. Theor. Polym. Sci.*, 1998, **8**(1–2), 229–246.
27 R. J. Messinger, T. G. Marks, S. S. Gleiman, F. Milstein and B. F. Chmelka, Molecular Origins of Macroscopic Mechanical Properties of Elastomeric Organosiloxane Foams, *Macromolecules*, 2015, **48**(14), 4835–4849.
28 S. Hamdani, C. Longuet, D. Perrin, J. M. Lopez-Cuesta and F. Ganachaud, Flame Retardancy of Silicone-Based Materials, *Polym. Degrad. Stab.*, 2009, **94**, 465–495.
29 X. Michalet, Mean square Displacement Analysis of Single-Particle Trajectories with Localization Error: Brownian Motion in an Isotropic Medium, *Phys. Rev. E*, 2010, **82**(4), 041914.
30 G. Z. Guo, J. N. Zhang, X. Chen, X. F. Zhao, J. B. Deng and G. J. Zhang, Molecular-Dynamics Study on the Thermodynamic Properties of Nano-SiO2 Particle-Doped Silicone Rubber Composites, *Comput. Mater. Sci.*, 2022, **212**, 111571.
31 G. A. Heiser, *Molecular Dynamics Calculation of Mean Square Displacement in Alkali Metals and Rare Gas Solids and Comparison with Lattice Dynamics*, Master's thesis, Brock University, 1984.
32 S. G. Charati and S. A. Stern, Diffusion of Gases in Silicone Polymers: Molecular Dynamics Simulations, *Macromolecules*, 1998, **31**(16), 5529–5535.
33 F. Melzer, R. Breuer, R. Dahlmann and C. Hopmann, Calculating Diffusion Coefficients from Molecular Dynamics Simulations for Foam Extrusion Modelling of Polypropylene with CO2, N2 and Ethanol, *J. Cell. Plast.*, 2022, **58**(4), 603–622.
34 L. Tao, J. L. He, T. Arbaugh, J. R. McCutcheon and Y. Li, Machine Learning Prediction on the Fractional Free Volume of Polymer Membranes, *J. Membr. Sci.*, 2023, 121131.
35 D. Turnbull and M. H. Cohen, Free-Volume Model of the Amorphous Phase: Glass Transition, *J. Chem. Phys.*, 1961, **34**(1), 120–125.
36 Y. Wang, Q. Wei, S. Wang, W. Chai and Y. Zhang, Structural and Water Diffusion of Poly (Acryl Amide)/poly (Vinyl Alcohol) Blend Films: Experiment and Molecular Dynamics Simulations, *J. Mol. Graphics Modell.*, 2017, **71**, 40–49.
37 Y. L. Luo, R. G. Wang, S. H. Zhao, Y. Y. Chen, H. F. Su, L. Q. Zhang, T. W. Chan and S. Z. Wu, Experimental Study and Molecular Dynamics Simulation of Dynamic Properties and Interfacial Bonding Characteristics of Graphene/Solution-Polymerized Styrene-Butadiene Rubber Composites, *RSC Adv.*, 2016, **6**, 58077–58087.
38 P. S. Sarath, G. Moni, J. J. George, J. T. Haponiuk, S. Thomas and S. C. George, A Study on the Influence of Reduced Graphene Oxide on the Mechanical, Dynamic Mechanical and Tribological Properties of Silicone Rubber Nanocomposites, *J. Compos. Mater.*, 2021, **55**(15), 2011–2024.

39 H. Zhang, F. Cai, Y. Luo, X. Yu and S. Wu, Grafting Silica onto Reduced Graphene Oxide via Hydrosilylation for Comprehensive Rubber Applications: Molecular Simulation and Experimental Study, *Polym. Compos.*, 2022, **43**(8), 5332–5343.

40 Y. S. Guo, J. Liu, Y. L. Lu, D. Dong, W. F. Wang and L. Q. Zhang, A Combined Molecular Dynamics Simulation and Experimental Method to Study the Compatibility Between Elastomers and Resins, *RSC Adv.*, 2018, **8**, 14401.

41 Z. P. Zhang, P. J. Tian, Z. F. Wang, Y. Yang, S. Y. Zhang and J. J. Xia, Experimental Studies and Molecular Dynamics Simulation of the Compatibility Between Thermoplastic Polyurethane Elastomer (TPU) and Asphalt, *Constr. Build. Mater.*, 2024, **411**, 134316.

42 C. Y. Li and A. Strachan, Cohesive Energy Density and Solubility Parameter Evolution During the Curing of Thermoset, *Polymer*, 2018, **135**, 162–170.

43 K. K. Shimizu, M. Tariq, M. F. C. Gomes, L. P. N. Rebelo and J. N. C. Lopes, Assessing the Dispersive and Electrostatic Components of the Cohesive Energy or Ionic Liquids using Molecular Dynamics Simulations and Molar Refraction Data, *J. Phys. Chem. B*, 2010, **114**(17), 5831–5834.

44 P. Becher, The Calculation of Cohesive Energy Density From the Surface Tension of Liquids, *J. Colloid Interface Sci.*, 1972, **38**(2), 291–293.

45 Y. Masubuchi, T. Kida, Y. Doi and T. Uneyama, Radial Distribution Functions of Entanglements in Primitive Chain Network Simulations, *Nihon Reoroji Gakkaishi*, 2021, **49**(5), 337–345.

46 E. Tsuchida, Revisiting the Minimum Image Locus Method for Calculating the Radial Distribution Functions, *Comput. Theor. Chem.*, 2023, **1227**, 114256.

47 H. Reiss and R. V. Casbreg, Radical Distribution Function of Small Hard Spheres from Scaled Particle Theory, and An Improved Equation of State, *J. Chem. Phys.*, 1974, **61**(3), 1107–1114.

48 A. Ozcan, R. Semino, G. Maurin and A. O. Yazaydin, Modeling of Gas Transport Through Polymer/MOF Interfaces: A Microsecond-Scale Concentration Gradient-driven Molecular Dynamics Study, *Chem. Mater.*, 2020, **32**(3), 1288–1296.

49 H. Tobita, Effect of Branch Point Distribution on the Radius of Gyration in Batch Free-Radical Polymerization with Chain Transfer to Polymer, *Macromol. Theory Simul.*, 2021, **30**(3), 2000036.

50 M. Y. Lobanov, N. S. Bogatyreva and O. V. Galzitskaya, Radius of Gyration as an Indicator of Protein Structure Compactness, *Mol. Biol.*, 2008, **42**, 623–628.

51 J. Cantarella, T. Deguchi, C. Shonkwiler and E. Uehara, Radius of Gyration, Contraction Factors, and Subdivisions of Topological Polymers, *J. Phys. A: Math. Theor.*, 2022, **55**(47), 475202.

52 J. Y. Mane and S. R. Stoyanov, Molecular Dynamics Simulations of the Oil Spill-Treating Phase-Selective Organogelator N-acetyl-L-isoleucine-N'-n-octyl Amide, *J. Mol. Liq.*, 2024, **397**, 123960.

53 D. N. Theodorou and U. W. Suter, Atomistic Modeling of Mechanical Properties of Polymeric Glasses, *Macromolecules*, 1986, **19**(1), 139–154.

54 S. Xi, M. Y. Cui, Q. W. Gao, S. L. Zhao and X. F. Xu, Mechanical Properties of Polybutadiene Rubber with Oxidation Defects: from Molecular Simulations, *Ind. Eng. Chem. Res.*, 2023, **62**(40), 16447–16455.

55 T. Raaska, S. Niemela and F. Sundholm, Atom-Based Modeling of Elastic Constants in Amorphous Polystyrene, *Macromolecules*, 1994, **27**(20), 5751–5757.

56 K. Rajabi and Sh. Hosseini-Hashemi, Application of the Generalized Hooke's Law for Viscoelastic Materials (GHVMs) in Nonlocal Free Damped Vibration Analysis of Viscoelastic Orthotropic Nanoplates, *Int. J. Mech. Sci.*, 2017, **124–125**, 158–165.

57 P. Kulkarni, B. Jose, S. Sambhudevan and B. Shankar, Influence of SiC and TiO2 on the Cure Characteristics and Mechanical Properties of Natural Rubber Composites, *Mater. Today: Proc.*, 2020, **46**, 4451–4453.

58 J. H. Weiner, *Statistical Mechanics of Elasticity*, Dover Publications, Com, New York, 1983.

59 A. Shokuhfar and B. Arab, The Effect of Cross linking Density on the Mechanical Properties and Structure of the Epoxy Polymers: Molecular Dynamics Simulation, *J. Mol. Model.*, 2013, **19**(9), 3719–3731.

60 L. Guo, H. Y. Xu, N. H. Wu, S. Yuan, L. J. Zhou, D. Y. Wang and L. J. Wang, Molecular Dynamics Simulation of the Effect of the Thermal and Mechanical Properties of Addition Liquid Silicone Rubber Modified by Carbon Nanotubes with Different Radii, *e-Polymers*, 2023, **23**, 20228105.

61 D. K. Singaravel, S. Sharma, P. Kumar and P. R. Patel, Effect of Functionalization and Defects in Carbon Nanotube on Mechanical Properties and Creep Behavior of Nitrile Butadiene Rubber Composites: A Molecular Dynamics Approach, *Polym.-Plast. Technol. Mater.*, 2023, **62**(15), 1998–2014.

62 D. E. Waller and X. Y. Xie, Hydrophilically Modified Curable Silicone Impression Material, *US Pat.*, US6201038, 2001.